A mechanistic study of the homogeneous catalytic hydroformylation of formaldehyde: synthesis and characterization of model intermediates

Albert S.C. Chan*

Department of Chemistry, National Chung Hsing University, Taichung (Taiwan, ROC);
Department of Chemistry, Hong Kong University of Science and Technology, Hong Kong, and Department of Applied Biology and Chemical Technology, Hong Kong Polytechnic, Hong Kong (Hong Kong)

Huey-sheng Shieh

Monsanto Corporate Research, St Louis, MO (USA)

(Received September 28, 1993; revised November 25, 1993)

Abstract

The homogeneous catalytic hydroformylation of formaldehyde is an important reaction in the pursuit of using syngas as a building block for higher valued chemicals. In this study we investigated the mechanism of the rhodium-catalyzed, base-promoted hydroformylation of formaldehyde through the syntheses and characterization of model complexes which illustrated the structures and the relevant chemistry of the key intermediates in the catalytic cycle. In the study of the rhodium model species, the rhodium alkyl species, $CH_3OCH_2Rh(CO)_2(PPh_3)_2$, could not be intercepted because of a very rapid CO insertion into the rhodium alkyl bond. The resulting rhodium acyl complex, $CH_3OCH_2C(O)Rh(CO)_2(PPh_3)_2$, was stable enough to be characterized by FT-IR. When iridium complexes were used as models, all important catalytic intermediates including the anionic catalyst ($[Ir(CO)_3PPh_3]^-$), the iridium alkyl species ($CH_3OCH_2Ir(CO)_2(PPh_3)_2$), and the iridium acyl species ($CH_3OCH_2C(O)Ir(CO)_2(PPh_3)_2$) were synthesized and unambiguously characterized. This model study clearly illustrated the novel anionic mechanism in the rhodium- or iridium-catalyzed, base-promoted hydroformylation of formaldehyde. The structural information obtained in this study is also important for the understanding of the mechanism of the hydroformylation reactions in general.

Key words: Crystal structures; Catalysis; Hydroformylation; Rhodium complexes; Alkyl complexes; Carbonyl complexes

Introduction

Synthesis gas is potentially one of the most economical raw materials for the manufacture of commodity chemicals [1]. In the pursuit of using syngas as a raw material for large-volume chemicals, a good target is ethylene glycol.

$$2CO + 3H_2 \longrightarrow HOCH_2CH_2OH \quad (1)$$

During the 1970s and early 1980s when oil prices were escalating, there were strong research efforts in converting syngas directly to ethylene glycol [2–4]. However, the severe reaction conditions required in this reaction rendered the approach economically unattractive. Later on, several mechanistic studies indicated that the rate-limiting step in the catalytic conversion of syngas to ethylene glycol was the formation of formaldehyde (or a formyl species) from syngas [5–7]. Since this step was thermodynamically unfavorable, very high concentrations of the precious metal catalysts and very high operating pressures were required to drive the reaction forward. Alternatively, a more practical approach was to convert syngas to methanol and then to formaldehyde, using well established heterogeneous catalysts. A key reaction in this approach was the hydroformylation of formaldehyde [8–14].

$$H_2CO + H_2 + CO \xrightarrow{\text{catalyst}} HOCH_2CHO \quad (2)$$

The glycolaldehyde product can be hydrogenated to ethylene glycol using established hydrogenation cata-

*Author to whom correspondence should be addressed.

SSDI 0020-1693(94)03800-4

lysts. Alternatively it can also be converted to higher-value-added products such as serine (via Strecker synthesis).

In our previous study of the rhodium-catalyzed hydroformylation of formaldehyde, we observed a profound effect of Lewis bases on the reaction rate [8]. A novel mechanism involving an anionic catalyst was proposed (Fig. 1) [15].

An *in situ* IR study of the catalytic reaction showed the presence of $HRh(CO)_2(PPh_3)_2$, $[Rh(CO)_4]^-$ and $[Rh(CO)_3(PPh_3)]^-$ under reaction conditions. This observation revealed the possibility that the rate-limiting step in the catalytic cycle was the nucleophilic attack of the formaldehyde by the anionic catalyst. (The subsequent reactions in the catalytic cycle were much faster and the intermediates formed after the rate-limiting step could not be detected.) This proposed mechanism was also supported by a preliminary kinetic study [16].

To fully illustrate the chemistry relevant to the catalytic cycle, it was important to synthesize the metal–alkyl and metal–acyl species, e.g. CH_3OCH_2–$M(CO)_2(PPh_3)_2$ and $CH_3OCH_2C(O)$–$M(CO)_2(PPh_3)_2$ (M = Rh or Ir) independently and to study their reactions. The reason for using the CH_3OCH_2 group to mimic the $HOCH_2$ ligand in the model complexes was to avoid the decomposition of the metal–alkyl species via β-hydride abstraction.

$$HOCH_2\text{–}Rh(CO)_2(PPh_3)_2 \longrightarrow HRh(CO)_2(PPh_3)_2 + CH_2{=}O \quad (3)$$

Results and discussion

Our original attempt in this study was to allow the anionic rhodium complexes ($[Rh(CO)_4]^-$ and $[Rh(CO)_3(PPh_3)]^-$ [17] to react with CH_3OCH_2Cl so as to generate the metal–alkyl species, $CH_3OCH_2Rh(CO)_x(PPh_3)_{4-x}$. The nucleophilic displacement of the chloride by the anionic complexes was quite facile at ambient temperature. However, the resulting rhodium–alkyl species, $CH_3OCH_2Rh(CO)_x(PPh_3)_{4-x}$, was not stable enough to be observed under the reaction conditions. A fast CO insertion generated the expected metal–acyl species, $CH_3OCH_2C(O)$–$Rh(CO)_2(PPh_3)_2$ (ν(CO) = 1986, 1941, 1663 cm^{-1}) in essentially quantitative yield [18]. These reactions are summarized in eqns. (4)–(7).

$$[Rh(CO)_4]^- + CH_3OCH_2Cl \xrightarrow{-Cl^-} CH_3OCH_2Rh(CO)_4 \quad (4)$$

$$CH_3OCH_2Rh(CO)_4 \xrightarrow[+2PPh_3]{\text{CO insertion}} CH_3OCH_2\overset{O}{\overset{\|}{C}}Rh(CO)_2(PPh_3)_2 \quad (5)$$

$$[Rh(CO)_3(PPh_3)]^- + CH_3OCH_2Cl \xrightarrow{-Cl^-} CH_3OCH_2Rh(CO)_3PPh_3 \quad (6)$$

$$CH_3OCH_2Rh(CO)_3PPh_3 \xrightarrow[+PPh_3]{\text{CO insertion}} CH_3OCH_2\overset{O}{\overset{\|}{C}}Rh(CO)_2(PPh_3)_2 \quad (7)$$

These observations were consistent with our proposed mechanism. However, for a more complete understanding of the catalytic cycle, it was of interest to synthesize the corresponding iridium complexes and to study their relevant chemistry. An important advantage of using iridium species was that they were kinetically more stable (the CO insertion was slower) and consequently the desired complexes could be isolated and characterized in a more convenient manner. Since the chemistry of the iridium complexes was quite similar to that of the corresponding rhodium species, the modeling of the rhodium intermediates with iridium analogs was also most intimate.

The first step in our modeling study with iridium species was to prepare the anionic iridium complexes and to compare them with the corresponding rhodium species. In this regard we reduced $IrCl(CO)(PPh_3)_2$ under the same conditions as in the preparation of the anionic rhodium complexes [17]. When $IrCl(CO)(PPh_3)_2$ was reduced with sodium amalgam in tetrahydrofuran under CO atmosphere, $[Ir(CO)_4]^-$ was found to be the dominant product (>95%, ν(CO) = 1894 cm^{-1}). Only a trace amount of $[Ir(CO)_3(PPh_3)]^-$ (ν(CO) = 1926, 1861 cm^{-1}) was observed. This trans-

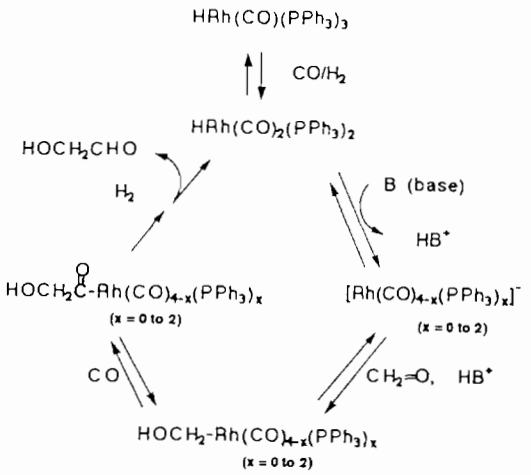

Fig. 1 A proposed mechanism of the hydroformylation of formaldehyde involving anionic rhodium catalysts.

formation closely resembled the reduction of the corresponding rhodium species [17].

$$IrCl(CO)(PPh_3)_2 \xrightarrow[THF,\ CO]{Na-Hg} \underset{(>95\%)}{[Ir(CO)_4]^-} + \underset{(<5\%)}{[Ir(CO)_3(PPh_3)]^-} \quad (8)$$

The fact that $[Ir(CO)_4]^-$ was the dominant species in this reaction was clearly due to the electronic effect of the anionic complex. In the anionic state, the electron-rich Ir(−1) species was stabilized by electron-withdrawing ligands. With a strong dative π-bonding capacity, the carbonyl ligands served this purpose much better than donor ligands such as triphenylphosphine.

When a solution of these anionic iridium species was stirred under a dinitrogen atmosphere at ambient temperature for several weeks, one of the carbonyl ligands in $[Ir(CO)_4]^-$ was replaced by a free triphenylphosphine ligand from the solution to yield $[Ir(CO)_3(PPh_3)]^-$.

$$[Ir(CO)_4]^- + PPh_3 \xrightarrow[\text{inert atmosphere}]{-CO,\ \text{slow}} [Ir(CO)_3(PPh_3)]^- \quad (9)$$

The sodium salt of this complex did not crystallize out of the solution easily. To prepare crystals of this species with the quality suitable for a single crystal X-ray diffraction study, a crown ether was added to the solution to trap the sodium cation. When a slight excess of 18-crown-6 ether was added to the THF solution of $Na[Ir(CO)_3(PPh_3)]$, the sodium cation was immediately complexed by the crown ether. Upon addition of excess of diethyl ether into this solution, crystals of crown ether-complexed sodium tricarbonyl(triphenylphosphine)iridate were obtained. The molecular structure of this complex was determined by X-ray diffraction to be identical to that of its rhodium analog [17] (Fig. 2).

The synthesis and characterization of the anionic iridium complexes supported our rationale of using iridium complexes as models for their rhodium analogs. The next step was to use the anionic iridium complexes to prepare the metal–alkyl and metal–acyl species to mimic the key intermediates in the catalytic cycle.

When the anionic iridium complexes (which were obtained by reducing $IrCl(CO)(PPh_3)_2$ with sodium amalgam under CO atmosphere) were allowed to react with CH_3OCH_2Cl in tetrahydrofuran, CH_3OCH_2–$Ir(CO)_2(PPh_3)_2$ (ν(CO) = 1971, 1921 cm^{-1}) was formed immediately.

$$[Ir(CO)_4]^- + CH_3OCH_2Cl \xrightarrow{-Cl^-} CH_3OCH_2{-}Ir(CO)_4 \xrightarrow[-2CO]{+2PPh_3} CH_3OCH_2{-}Ir(CO)_2(PPh_3)_2 \quad (10)$$

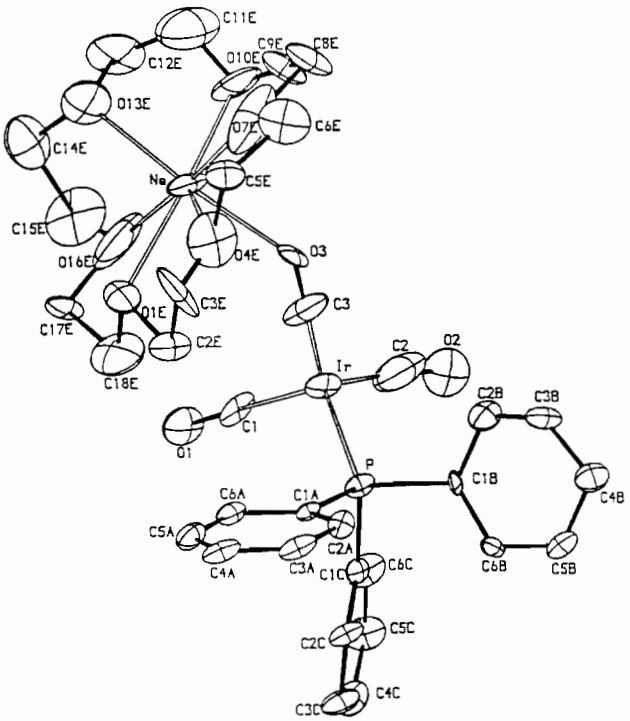

Fig. 2. A perspective view of $[Na(C_{12}H_{24}O_6)][Ir(CO)_3(PPh_3)]$. Selective bond lengths (Å): Ir–C1 = 1.86(2); Ir–C2 = 1.82(4); Ir–C3 = 1 83(3); Ir–P = 2 305(5); Na–O3 = 2 48(3), Na–O1E = 2 56(3); Na–O4E = 2.88(3); Na–O7E = 2 49(3); Na–O10E = 2 34(3); Na–O13E = 2 47(3); Na–O16E = 2 51(3) Selected bond angles (°) C1–Ir–C2 = 112(1); C1–Ir–C3 = 107(1); C1–Ir–P = 106(1), C2–Ir–C3 = 119(2), C2–Ir–P = 102(1), C3–Ir–P = 110 4(7)

$$[Ir(CO)_3PPh_3]^- + CH_3OCH_2Cl \xrightarrow{-Cl^-} CH_3OCH_2{-}Ir(CO)_3PPh_3 \xrightarrow[-CO]{+PPh_3} CH_3OCH_2{-}Ir(CO)_2(PPh_3)_2 \quad (11)$$

The generation of CH_3OCH_2–$Ir(CO)_2(PPh_3)_2$ from CH_3OCH_2–$Ir(CO)_4$ and from CH_3OCH_2–$Ir(CO)_3(PPh_3)$ was due to the electronic effect of the complexes. In contrast to the anionic iridium species which preferred electron-withdrawing ligands such as CO, the neutral complexes were more stable with a balance of donor ligands. Consequently a rapid ligand exchange generated the desired CH_3OCH_2–$Ir(CO)_2(PPh_3)_2$ complex after the nucleophilic chloride displacement by the anionic complexes. White crystals of CH_3OCH_2–$Ir(CO)_2(PPh_3)_2$ were obtained when petroleum ether was slowly added to a THF solution of this complex. A single crystal X-ray diffraction study of this complex revealed a distorted trigonal bipyramidal structure (Fig. 3).

Once the key metal–alkyl species, $CH_3OCH_2Ir(CO)_2$-$(PPh_3)_2$, was isolated and unambiguously characterized,

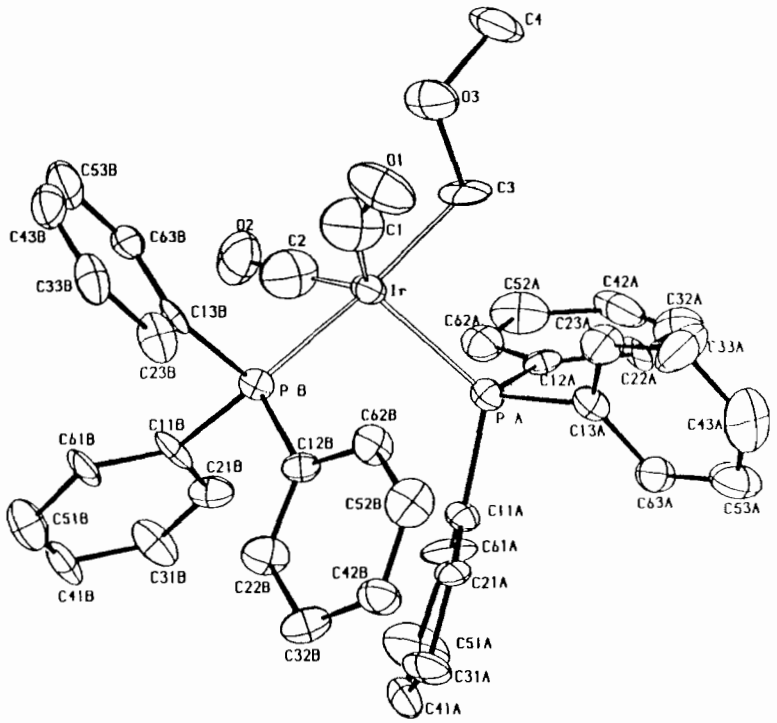

Fig 3 A perspective view of CH_3OCH_2–$Ir(CO)_2(PPh_3)_2$. Selected bond lengths (Å): Ir–C1 = 1.80(4), Ir–C2 = 1.53(4), Ir–C3 = 2 12(2); Ir–PA = 2.374(6), Ir–PB = 2.366(6) Selected bond angles (°): C1–Ir–C2 = 115(2); C1–Ir–C3 = 90(1); C1–Ir–PA = 129(1); C1–Ir–PB = 83(1), C2–Ir–C3 = 119(2); C2–Ir–PA = 117(1), C2–Ir–PB = 82(1); C3–Ir–PA = 82.5(6); C3–Ir–PB = 172.8(7), PA–Ir–PB = 103 5(2).

It was of significant interest to study the subsequent CO insertion step which was important in the catalytic reaction. When a solution of $CH_3OCH_2Ir(CO)_2(PPh_3)_2$ was pressurized with CO, the expected CO insertion was indeed observed. Both $CH_3OCH_2C(O)Ir(CO)_2(PPh_3)_2$ (ν(CO) = 1972, 1928, 1654 cm^{-1}) and $CH_3OCH_2C(O)Ir(CO)_3(PPh_3)$ (ν(CO) = 2047, 1983, 1673 cm^{-1}) were obtained, depending on the conditions. In fact, the inter-conversion of these three species closely resembled the corresponding reaction intermediates in the catalytic cycle.

$$CH_3OCH_2Ir(CO)_2(PPh_3)_2 \underset{-CO}{\overset{+CO}{\rightleftharpoons}} CH_3OCH_2C(O)Ir(CO)_2(PPh_3)_2$$

$$+CO \Big\uparrow\Big\downarrow -CO \qquad -PPh_3 \Big\downarrow\Big\uparrow +PPh_3 \qquad (12)$$

$$CH_3OCH_2C(O)Ir(CO)_3(PPh_3)$$

$CH_3OCH_2C(O)Ir(CO)_2(PPh_3)_2$ and $CH_3OCH_2C(O)$-$Ir(CO)_3(PPh_3)$ were also independently synthesized by reacting $CH_3OCH_2C(O)Cl$ with a solution of the anionic iridium species (which were obtained by reducing $IrCl(CO)(PPh_3)_2$ with sodium amalgam under CO atmosphere.)

$$[Ir(CO)_4]^- + CH_3OCH_2C(O)Cl \xrightarrow{-Cl^-}$$

$$CH_3OCH_2C(O)—Ir(CO)_4$$

$$PPh_3 \Big\downarrow\Big\uparrow \qquad (13)$$

$$CH_3OCH_2C(O)—Ir(CO)_2(PPh_3)_2$$

$$+$$

$$CH_3OCH_2C(O)—Ir(CO)_3(PPh_3)$$

Single crystals of $CH_3OCH_2C(O)$–$Ir(CO)_2(PPh_3)_2$ were isolated when diethylether was slowly added to its THF solution. The molecular structure of this complex was determined by X-ray diffraction to be a distorted trigonal bipyramid (Fig. 4). It is noteworthy that the unambiguous characterization of these iridium–alkyl and iridium–acyl species enabled a complete modeling of all the key intermediates in the catalytic cycle.

When a THF solution containing CH_3-$OCH_2C(O)$–$Ir(CO)_2(PPh_3)_2$, $CH_3OCH_2C(O)$–$Ir(CO)_3$-(PPh_3) and PPh_3 was exposed to H_2 or CO/H_2 atmosphere, $CH_3OCH_2C(O)H$ and $HIr(CO)_2(PPh_3)_2$ were obtained. This reaction completed the modeling of the catalytic cycle for the hydroformylation of formaldehyde.

In conclusion, by using suitable rhodium and iridium complexes and by monitoring their appropriate reactions, we were able to model all the key intermediates in the catalytic cycle for the rhodium-catalyzed, base-

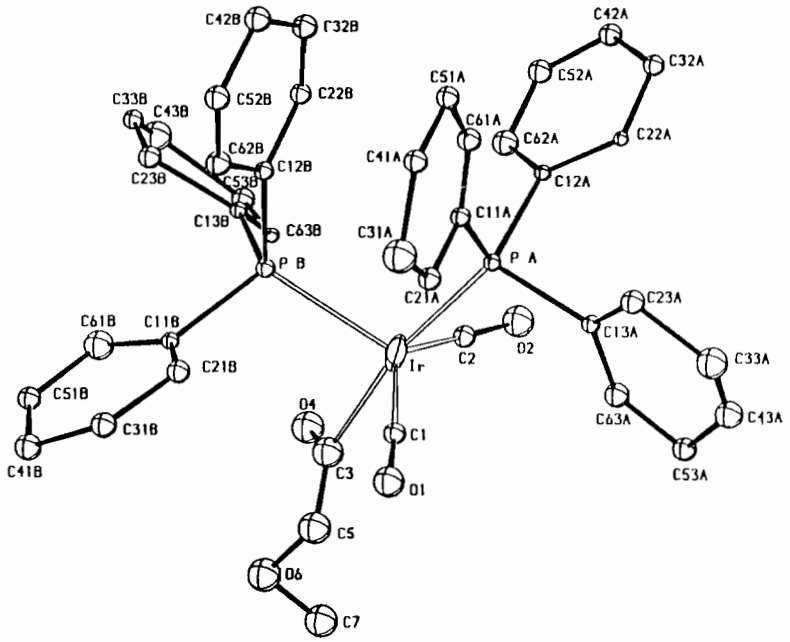

Fig. 4. A perspective view of $CH_3OCH_2C(O)$–$Ir(CO)_2(PPh_3)_2$. Selected bond lengths (Å): Ir–C1 = 1.86(2); Ir–C2 = 1.84(2); Ir–C3 = 2.08(1); Ir–PA = 2.372(3); Ir–PB = 2.381(3). Selected bond angles (°): C1–Ir–C2 = 134.8(7); C1–Ir–C3 = 86.0(6); C1–Ir–PA = 89 4(4); C1–Ir–PB = 114.6(5); C2–Ir–C3 = 86.4(7); C2–Ir–PA = 90.4(5); C2–Ir–PB = 109.6(5); C3–Ir–PA = 169.(4); C3–Ir–PB = 88 2(4), PA–Ir–PB = 102.1(1).

promoted hydroformylation of formaldehyde. From a broader perspective, these complexes were also good models to illustrate the structures of the important intermediates in the general, rhodium-catalyzed, hydroformylation reactions.

Experimental

General data

Unless indicated, all operations were carried out under N_2 in an inert atmosphere box. All reagents were purified according to standard, published methods and degassed before use. IR spectra were recorded on a Nicolet MX-1 spectrometer. X-ray crystallographic data were collected on a Syntex $P2_1$ automated diffractometer.

Isolation of single crystals of 18-crown-6 ether-complexed sodium tricarbonyl(triphenylphosphine)iridate

A 100 ml Fisher-Porter bottle was charged with 0.5 g $IrCl(CO)(PPh_3)_2$, 50 g 1% sodium amalgam, 30 ml THF and a magnetic stirrer. The mixture was stirred under 50 psig CO at 60 °C for 20 h. After the solution was cooled to ambient temperature, the CO was vented and the solution was decanted and filtered under an N_2 atmosphere. The clear, light yellow solution was refluxed under an N_2 atmosphere for 24 h and then cooled to ambient temperature. The resulting solution was transferred to a 4 ounce glass bottle. Into this solution was added 0.25 g 18-crown-6 ether and the mixture was shaken well to make a homogeneous solution. Three small test tubes which were filled with diethyl ether were placed inside the bottle. (The level of the iridium solution was at about one-third of the height of the test tubes.) The bottle was then capped tightly and placed inside an inert atmosphere box to allow the diethyl ether to diffuse into the THF solution. After two days, yellow crystals were found to deposit at the bottom of the bottle. The solution was decanted and the crystals were carefully rinsed with diethyl ether. Good quality crystals were chosen to be mounted and sealed in capillary tubes for X-ray diffraction measurement.

Isolation of single crystals of CH_3OCH_2–$Ir(CO)_2(PPh_3)_2$

A 100 ml Fisher-Porter bottle was charged with 0.5 g $IrCl(CO)(PPh_3)_2$, 50 g 1% sodium amalgam, 30 ml THF and a magnetic stirrer. The mixture was stirred under 50 psig CO at 60 °C for 20 h. After the solution was cooled to ambient temperature, the CO was vented and the solution was decanted. The solution was allowed to react with 0.1 g CH_3OCH_2Cl and the final mixture was filtered under an N_2 atmosphere. The clear, light yellow filtrate was transferred to a 4 ounce glass bottle. Three small test tubes which were filled with petroleum ether were placed inside the bottle. (The level of the iridium solution was at about one-third of the height of the test tubes.) The bottle was

TABLE 1. Crystallographic data

	$[Na(C_{12}H_{24}O_6)][Ir(CO)_3(PPh_3)]$	CH_3OCH_2–$Ir(CO)_2(PPh_3)_2$	CH_3OCH_2CO–$Ir(CO)_2(PPh_3)_2$
Formula	$C_{33}H_{39}O_9NaPIr$	$C_{40}H_{35}O_3P_2Ir$	$C_{41}H_{35}O_4P_2Ir$
Molecular weight	825 8	817.87	845.88
a (Å)	10.867(3)	10.733(2)	10.495(5)
b (Å)	13.124(3)	17 001(2)	11.658(6)
c (Å)	13 148(3)	19 327(3)	16 312(3)
α (°)	73 75(2)	87.16(1)	104.52(3)
β (°)	72.07(2)	86.74(1)	93 26(3)
γ (°)	88.35(2)	88 03(1)	111.85(3)
V (Å^3)	1709.4(7)	3514 6(9)	1768(1)
Z	2	4	2
D_{calc} (g/cm^3)	1.60	1.54	1 59
Space group	$P\bar{1}$	$P\bar{1}$	$P\bar{1}$
$F(000)$	824	1624	840
Crystal shape	rectangular prism	rectangular prism	rectangular prism
Crystal color	yellow greenish	colorless	pale yellow
Crystal size (mm)	$0.5\times0.2\times0.2$	$0\,2\times0.3\times0.5$	$0.4\times0.2\times0.2$
μ (cm^{-1})	84 66(Cu)	37.08(Mo)	83.65(Cu)
Diffractometer	Syntex $P2_1$	Syntex $P2_1$	Syntex $P2_1$
Scan type	θ–2θ	θ–2θ	θ–2θ
Scan rate (°/min)	2–19.5	2–19 5	2–19.5
$2\theta_{max}$ (°)	120 (Cu Kα)	50 (Mo Kα)	120 (Cu Kα)
Temperature (°C)	−140	23	23
No. unique reflections	4974	13179	5141
No. reflections with $I \geq 2.33\sigma(I)$	4020	6692	4682
No. of variables	406	416	198
R (obs. reflections)	0 1158	0 0804	0.1336
R_w (obs. reflections)	0.1554	0 0782	0.1655
Goodness of fit	7.316	2 808	4.387

then capped tightly and placed inside an inert atmosphere box to allow the petroleum ether to diffuse into the THF solution. After two days, crystals were found to deposit at the bottom of the bottle. The solution was decanted and the crystals were carefully rinsed with petroleum ether. Good quality crystals were chosen to be mounted and sealed in capillary tubes for X-ray diffraction measurement.

Isolation of single crystals of $CH_3OCH_2C(O)Ir(CO)_2(PPh_3)_2$

A 100 ml Fisher-Porter bottle was charged with 0.5 g $IrCl(CO)(PPh_3)_2$, 50 g 1% sodium amalgam, 30 ml THF and a magnetic stirrer. The mixture was stirred under 50 psig CO at 60 °C for 20 h. After the solution was cooled to ambient temperature, the CO was vented and the solution was decanted. The solution was allowed to react with 0.1 g $CH_3OCH_2C(O)Cl$ and the final mixture was filtered under an N_2 atmosphere. The clear, light yellow filtrate was transferred to a 4 ounce glass bottle. Three small test tubes which were filled with diethyl ether were placed inside the bottle. (The level of the iridium solution was at about one-third of the height of the test tubes.) The bottle was then capped tightly and placed inside an inert atmosphere box to allow the diethyl ether to diffuse into the THF solution. After two days, crystals were found to deposit at the bottom of the bottle. The solution was decanted and the crystals were carefully rinsed with diethyl ether. Good quality crystals were chosen to be mounted and sealed in capillary tubes for X-ray diffraction measurement.

X-ray crystallographic analysis of $[Na(C_{12}H_{24}O_6)][Ir(CO)_3(PPh_3)]$

The crystallographic data of $Na(C_{12}H_{24}O_6)][Ir(CO)_3(PPh_3)]$ are summarized in Table 1. The X-ray data were collected at low temperature (around −140 °C) with Cu Kα ($\lambda = 1.5418$ Å). The structure was solved by the Patterson heavy atom method and was refined by a block diagonal least-squares procedure. The refinement converged at a discrepancy R factor of 0.1158. The two highest peaks in the difference Fourier map at this stage had electron densities of 3.3 and 3.2 electron/cm^3, respectively, and were 0.6 Å away from the Ir position. This happened quite frequently when the diffraction data were not corrected for the crystal absorption effect. In this case, some Ψ scan data were used for the empirical absorption correction. The third and fourth highest peaks (2.5 and 2.1 electrons/cm^3) in the map revealed some disorder around the CO groups. The crown ether did not show any significant

disorder. No disorder model had been included in the refinement procedure. A perspective view and the numbering scheme of the structure are shown in Fig. 2.

X-ray crystallographic analysis of CH_3OCH_2–$Ir(CO)_2(PPh_3)_2$

The crystallographic data are summarized in Table 1. The X-ray diffraction data were collected at ambient temperature (around 23 °C) with Mo Kα ($\lambda = 0.7107$ Å). There were two molecules in each asymmetric unit. The first highest four peaks in the Patterson map were (0.4648, 0.5000, 0.0000) with weight 999; (0.5996, 0.8945, 0.4727) with weight 818.5; (0.1328, 0.3945, 0.4727) with weight 461.5; and (0.0332, 0.3945, 0.4727). This gave the two initial positions of Ir atoms (0.5167, 0.697, 0.2364) and (0.0664, 0.197, 0.2364). It is worth noting that the y and z coordinates in these two molecules are highly correlated. They are different by 0.5 in the y coordinate and are identical in the z coordinate. The structure was solved by using the phases based on the two Ir atoms. The structure was refined by a block diagonal least-squares procedure. The refinement converged at a discrepancy R factor of 0.0804. A disorder model, with the half occupied positions on C5CB, C6CB, C5EB and C6EB, had been included in the refinement procedure. A perspective view and the numbering scheme of the structure are shown in Fig. 3.

X-ray crystallographic analysis of $CH_3OCH_2C(O)$–$Ir(CO)_2(PPh_3)_2$

The crystallographic data are summarized in Table 1. The X-ray diffraction data were collected at room temperature (around 23 °C) with Cu Kα ($\lambda = 1.5418$ Å). The structure was solved by the Patterson heavy atom method and was refined by a block diagonal least-squares procedure. Throughout the refinement, only the Ir atom was kept in anisotropic temperature factors and all the rest were in isotropic temperature factors. The refinement converged at a discrepancy R factor of 0.1336. A perspective view and the numbering scheme of the structure are shown in Fig. 4.

Acknowledgements

We thank Dr D. Forster for helpful discussions. A.S.C. Chan also thanks the National Science Council of the Republic of China for a grant which supports his collaborative research in Taiwan.

References

1 National Research Council, *Opportunities in Chemistry*, National Academy Press, Washington, DC, 1985.
2 B.D Dombek, *Adv Catal*, *32* (1983) 325
3 J.F Knifton, *J. Am. Chem Soc*, *103* (1981) 3959.
4 M. Ishino, M. Tamura, T. Deguchi and S Nakamura, *J Catal*, *133* (1992) 325
5 H M. Feder and J W. Rathke, *Ann. N Y Acad Sci*, *333* (1980) 45.
6 W. Keim, M Berger and J Schlupp, *J Catal*, *61* (1980) 359
7 D.R. Fahey, *J. Am Chem Soc*, *103* (1981) 136
8 A.S.C. Chan, W.E. Carroll and D.E. Willis, *J Mol Catal.*, *19* (1983) 377.
9 A S C. Chan, (Monsanto), *US Patent No 4 477 685* (1984)
10 M. Marchionna and G. Longoni, *J Mol Catal.*, *57* (1989) 221
11 A.J. Spencer, *Organomet Chem*, *194* (1980) 113
12 R W Goetz (National Distiller), *US Patent No 4 200 765* (1980)
13 T Yukawa and H. Wakamatsu (Ajinomoto), *US Patent No 3 920 753* (1975).
14 T. Okano, M. Makino, H. Konoshi and J Kiji, *Chem Lett*, (1985) 1793.
15 A.S.C. Chan and H.S. Shieh, *Int Chem. Conf. Pacific Basin Soc*, *Honolulu, HI, USA, Dec 16–22, 1984*, Paper No. O3G22
16 A S.C Chan and P Mill, unpublished results.
17 A S.C. Chan, H.S. Shieh and J.R. Hill, *J Organomet Chem.*, *279* (1985) 171.
18 A.S.C Chan, *Inorg Chim Acta*, *210* (1993) 5